Astron. Astrophys. 332, 135–148 (1998)

ASTRONOMY
AND
ASTROPHYSICS

Modelling intermediate age and old stellar populations in the Infrared

A. Bressan[1], **G.L. Granato**[1], **and L. Silva**[2]

[1] Astronomical Observatory, Vicolo dell'Osservatorio 5, I-35122 Padova, Italy
[2] ISAS, Trieste, Via Beirut n.2-4, I-34013 Trieste, Italy

Received 9 July 1997 / Accepted 14 October 1997

Abstract. In this paper we have investigated the spectrophotometric properties of the Asymptotic Giant Branch (AGB) stars and their contribution to the integrated infrared emission in simple stellar populations (SSP). Adopting analytical relations describing the evolution of these stars in the HR diagram and empirical relations for the mass-loss rate and the wind terminal velocity, we were able to model the effects of the dusty envelope around these stars, with a minimal number of parameters. After deriving simple scaling relations which allow us to account for the metallicity of the star, we computed isochrones at different age and initial metal content. We compare our models with existing infrared colors of M giants and Mira stars and with IRAS PSC data. The former data are fairly well reproduced by our models, though a possible inadequacy of the adopted atmospheric models is indicated. Though being characterized by different metallicity, the isochrones follow a single path in the IRAS two color diagram, fixed by the composition and optical properties of the dust mixture. The bulk of the data in the latter diagram is delimited by the curves corresponding to a mixture of silicate grains and one of carbonaceous grains. We also discuss the effects of detached shells of matter but we do not take into account this phenomenon in the present computations.

Contrary to previous models, in the new isochrones the mass-loss rate, which establishes the duration of the AGB phase, also determines the spectral properties of the stars. The contribution of these stars to the integrated light of the population is thus obtained in a consistent way. We find that the emission in the mid infrared is about one order of magnitude larger when dust is taken into account in an intermediate age population, irrespective of the particular mixture adopted. The dependence of the integrated colors on the metallicity and age is discussed, with particular emphasis on the problem of age-metallicity degeneracy. We show that, contrary to the case of optical or near infrared colors, the adoption of a suitable pass-band in the mid infrared allows a fair separation of the two effects. We suggest intermediate redshift elliptical galaxies as possible targets of this method of solving the age-metallicity dilemma.

The new SSP models constitute a first step in a more extended study aimed at modelling the spectral properties of the galaxies from the ultraviolet to the far infrared.

Key words: stars: fundamental parameters; mass-loss; AGB and post-AGB – dust, extinction – galaxies: stellar content – infrared: stars

Send offprint requests to: A. Bressan (bressan@pd.astro.it)

1. Introduction

Effects of dust in the envelopes of Mira and OH/IR stars are usually neglected in the spectrophotometric synthesis of a composite population, on the notion that the contribution of dust enshrouded stars to the integrated bolometric light is negligible. While this can be justified in very old systems, it is not the case among intermediate age population clusters, whose brightest tracers are indeed the asymptotic giant branch stars. In these stars, the light absorbed by the dust at optical wavelengths is reemitted in a broad region from a few to a few hundred microns, where it overwhelms the stellar component. In addition to the thermal emission from the dust particles there are characteristic lines from molecules and often maser emission. Dust and molecular emission from these stars have been interpreted as a signature of an expanding circumstellar envelope, where gas particles reach the escape velocity giving rise to significant mass-loss (Salpeter 1974a,b, Goldreich & Scoville 1976, Elitzur et al. 1976). Mass loss measurements made by different authors and different techniques all agree with the notion that Mira and OH/IR stars constitute the final nuclear evolutionary phase where low and intermediate mass stars lose the whole envelope and turn toward the fate of a white dwarf. The process responsible of such a huge mass-loss is still unknown but, nowadays, there is a growing amount of evidence from both the observational and the theoretical point of view, that large amplitude pulsations coupled with radiation pressure on dust grains play a major role in determining the observed high mass-loss rates. From the observational side there exists a tight

correlation between the mass-loss rate and the period of pulsation, even if the role of the amplitude of pulsations has not yet been exploited (see Habing 1996 for a thorough review on the subject). On the other hand hydrodynamic models show that large amplitude pulsations may levitate matter out to a radius where radiation pressure on dust accelerates the gas beyond the escape velocity (Bowen & Willson 1991). Luminosity functions of AGB stars in well studied populous clusters and fields of the Large Magellanic Cloud (LMC) indicate that the mass loss along this phase is far larger than that predicted by the usual Reimers law which, on the contrary, successfully describes the evolution along the red giant branch in old systems. A super-wind phase (Fusi-Pecci & Renzini 1976) is often invoked to account for the paucity of bright AGB stars. A mass-loss rate exponentially increasing with time, naturally evolving into a super-wind phenomenon, is obtained both by the hydrodynamic models of Bowen & Willson (1991), due to the growth rate of the density scale height at the sonic point in the envelope, as well as by the semiempirical treatment of Vassiliadis and Wood (1993-VW), as a consequence of the growth rate of the period of pulsation as the star climbs along the AGB losing its mass. Finally only mass loss rates that include a super-wind phase, like those described above, can account for the relation between the initial stellar and final white dwarf mass (e.g. Weidemann 1987).

In spite of the tight link between the mass–loss rate and the infrared emission among these objects very few attempts have been made in providing a coherent picture of the photometric evolution of an AGB star toward its final fate. In particular existing isochrones do not account for the effects of dust and molecules around AGB stars and are inadequate to study the photometric properties of star clusters and galaxies when and/or where these stars contribute a significant fraction of the light. To cope with this difficulty we constructed a set of theoretical models which account for the effects of the circumstellar envelope and obtained a new set of theoretical isochrones particularly suited for the analysis of the infrared and mid infrared data.

We stress in advance that our viewpoint is different from that adopted in several previous studies devoted to the subject. Usually a physically sound model is constructed and fitted to the available observations in order to obtain the characteristic parameters of the model such as the dust mass-loss rate, the effective temperature, the grain composition and so on. The gas mass–loss rate follows from the assumption of a value of the dust–to–gas ratio, or alternatively this latter quantity is obtained when the gas mass–loss rate is directly estimated from other measurements. Models are thus applied and tuned to observations of specific objects. This ensemble of data constitutes a statistical basis for the parameterization of the mass–loss rate as a function of the period of the stars, a relation that has recently been widely adopted in model computations.

Here we will proceed along the opposite direction. We will assume that the mass–loss rate of AGB stars is known as a function of the basic stellar parameters (mass, luminosity, radius) either from hydrodynamic models (e.g. Bowen & Willson 1991) or from empirical relations (VW). For a given dust to gas ratio the mass-loss rate in dust is derived, and the spectrophotometric properties of the envelope are computed from the given stellar spectrum and from the geometry and velocity of the matter flow. A series of photometric envelope models is then computed for several different basic parameters and adopted whenever necessary in the construction of the isochrones, in order to obtain both the colors of the single stars and the integrated spectra.

The paper is organized as follows. Sect. 2 describes the envelope model. Adopting a spherically symmetric stationary flow of matter the radiative transport equation is solved to derive the extinction and the emission of the dust as a function of the wavelength. The reliability of the model is tested by comparing it to data assembled from the literature. A monoparametric class of models is constructed as a function of the optical depth of the envelope τ at 1μm (thereinafter τ_1) and a relation between the optical depth τ_1 and the basic stellar quantities (mass-loss rate, expansion velocity and luminosity) is obtained, in order to allow the interpolation between two different stellar envelopes.

Sect. 3 describes the construction of the isochrones in the theoretical HR diagram. Relations providing the mass-loss rate and the expansion velocity are adapted from Vassiliadis & Wood (1993) with some minor modifications suggested by the comparison of our envelope model with existing observations of stars in the Magellanic Clouds and in our galaxy: in both the super-wind mass-loss rate and the velocity period relation we include a suitable dependence on the metallicity.

In Sect. 4 we describe the spectrophotometric properties of the isochrones. For the evolutionary phases before the AGB, the method is identical to the one adopted by Bressan et al. (1994). Along the AGB the suitable envelope model is applied to the otherwise unaffected stellar spectrum and absorption and reemission by dust is then included in the model as it moves along the AGB phase. In this way we are able to obtain consistent isochrones and corresponding integrated spectra in the mid infrared dominion. We compare our isochrones of different ages and metallicity with the IRAS two color diagram and discuss the reliability of our sequence of envelope models. We briefly discuss the difficulty of a monoparametric sequence of envelopes with varying optical depth τ_1 to interpret the IRAS two color diagram, already encountered by other authors (Bedijn 1987, Ivezic & Elitzur 1995). The comparison with near infrared colors of a sample of M giants and Miras shows that the inclusion of the dust constitutes a significant improvement with respect to previous models.

Sect. 5 is devoted to the spectro-photometric integrated properties of the simple stellar populations (SSP). In particular we stress the difficulty to disentangle age and metallicity effects from the analysis of the optical and near IR colors alone. However we show that extending the colors to the mid infrared may solve the age-metallicity degeneracy at least in intermediate age systems. Possible targets where the new models should exploit their highest capabilities are thus intermediate redshift elliptical galaxies where the stellar populations are only few Gyr old.

2. The dust envelope model

Radiative transfer in dusty shells around "windy" stars has been previously considered by many authors (see Habing, 1996 and references therein). The most advanced approaches couple the radiative transfer and the hydrodynamic equations of motion for the two interacting fluids of the wind, the gas and the dust (Habing et al. 1994; Ivezic & Elitzur 1995). This is necessary to achieve a fully consistent solution, because the radiation pressure on dust grains is widely believed to be the main driver of the high $\dot{M}$ observed in OH/IR stars.

However our interest here is to "correct" the stellar spectra predicted by standard evolutionary tracks by including the effects of dusty envelopes associated with AGB mass-loss. We need therefore a recipe, consistent with available observations, to associate the fundamental parameters of the star, such as mass-loss, escape-velocity, luminosity, radius and metallicity, with the geometrical parameters of its dusty shell most relevant in determining the spectral effects. Along an isochrone the stellar parameters will change according to some specified relations that will be discussed in the following section, along with the procedure of assigning each point of the isochrone the most adequate envelope model. Here we will assume that the luminosity, the radius, the mass-loss rate, the escape velocity and the dust to gas ratio of the model are known, and we will derive the corresponding spectral properties of the dust envelope.

We adopt spherical symmetry and, in a first order picture, an outflow velocity $v_{\rm exp}$ independent of radius. Thus for a given $\dot{M}$, the dust density outside the sublimation radius r_{in} wherein the grains are supposed to form suddenly, scales as r^{-2}:

$$\rho_d(r) = \frac{\dot{M}\delta}{4\pi v_{\rm exp}} \frac{1}{r^2} \tag{1}$$

where δ is the assumed dust–to–gas mass ratio. The envelope extends out to a radius $r_{out} = 1000\, r_{in}$.

We also test the effects of the presence of an expanding 0.02 $M_\odot$ shell of matter superimposed to the standard r^{-2} law. However these effects will not be taken into account in our SSP models and are only meant to illustrate uncertainties brought about by transient phenomena. Adopting a gaussian profile for the density enhancement due to the annulus alone, centered at $r_a < r_{out}$ (the outer radius of the dust distribution) and with characteristic width Δr_a, the total dust density becomes

$$\rho_d(r) = \frac{\dot{M}\delta}{4\pi v_{\rm exp}} \frac{1}{r^2} \left[1 + f \times \; e^{-\left(\frac{r-r_a}{\Delta r_a}\right)^2} \right]. \tag{2}$$

It is straightforward to relate the constant f to the mass ΔM_a (=0.02 $M_\odot$) in the annulus:

$$\Delta M_a = \frac{\dot{M}\, f}{v_{\rm exp}} \int_{r_{in}}^{r_{out}} e^{-\left(\frac{r-r_a}{\Delta r_a}\right)^2} dr \tag{3}$$

To mimic an outward moving density enhancement, we computed three models with $\Delta r_a = 0.1\, r_{out}$ and $r_a = 0.2\, r_{out}$, $r_a = 0.5\, r_{out}$ and $r_a = 0.8\, r_{out}$. Note that the corresponding density enhancement barely affects the optical depth of the envelope, though it may affect the emission in a given spectral region. Indeed the fraction of column density due to the enhancement in the annulus is $\simeq 3 \times 10^{-2} f$, $\simeq 7 \times 10^{-4} f$ and $\simeq 3 \times 10^{-4} f$, respectively, for the three adopted values of r_a/r_{out}. On the other hand the mass–loss rates relevant for this paper are $\gtrsim 10^{-5} M_\odot$/yr while typical values of the outflow velocity are ≤ 20 km/s. Eq. 2 yields then $f \leq 5$ which means that the optical depth is always dominated by the standard r^{-2} term.

Table 1. Parameters of the adopted grain mixture.

Type	a [μm]	D [gr/cm^3]	X	T_s [K]
Mixture A				
Amorph. Sil. . .	0.1	2.50	0.781	1000
Silicate	0.03	2.50	0.189	1000
Silicate	0.01	2.50	0.030	1000
Mixture B				
Amorph. Carb.	0.1	2.26	0.398	1500
Graphite	0.03	2.26	0.258	1500
Graphite	0.01	2.26	0.344	1500

The parameters $\dot{M}$ and $v_{\rm exp}$ entering into Eq. 2 are derived from the fundamental stellar parameters as described in Sect. 3. The remaining problem is to estimate the dust to gas mass fraction δ. It is widely believed that the high mass loss rates in the AGB phase are driven by the transfer of momentum of photons to the dust grains and then to the gas. Therefore a close relationship between the dust abundance and the velocity of the flow is expected. The problem has been studied carefully by Habing et al. (1994), who confirmed that the terminal velocity of the gas flow $v_{\rm exp}$ depends rather strongly on δ. On the other hand they found also that the flow reaches rather quickly a velocity close to $v_{\rm exp}$, in keeping with our previous assumption, and that the difference between the dust and the gas velocity is positive and decreases with increasing $\dot{M}$. At the high mass loss rates mostly relevant for this work the two velocities are within 10 %, and the results by Habing et al. can be well approximated by the simple equation

$$\left(\frac{v_{\rm exp}}{21\,{\rm km/s}}\right) \simeq \left(\frac{L}{10^4 L_\odot}\right)^{0.35} \left(\frac{\delta}{10^{-2}}\right)^{0.5} \tag{4}$$

which can be inverted to yield

$$\delta \simeq 0.015\, v_{\rm exp}^2[{\rm km/s}] \left(\frac{L}{L_\odot}\right)^{-0.7} \tag{5}$$

This set of equations gives the dust density at each position in the dusty shell as a function of the stellar parameters. Dust grains absorb and scatter the stellar radiation, with an efficiency much greater in the optical-UV regime than in the IR, and reradiate the absorbed energy at IR wavelengths. At the high mass loss rates achieved in the super-wind phase, the involved densities imply that the dust emission is self-absorbed, and therefore to compute the emitted spectrum the radiative transfer problem must be solved. The numerical code we use is described in detail

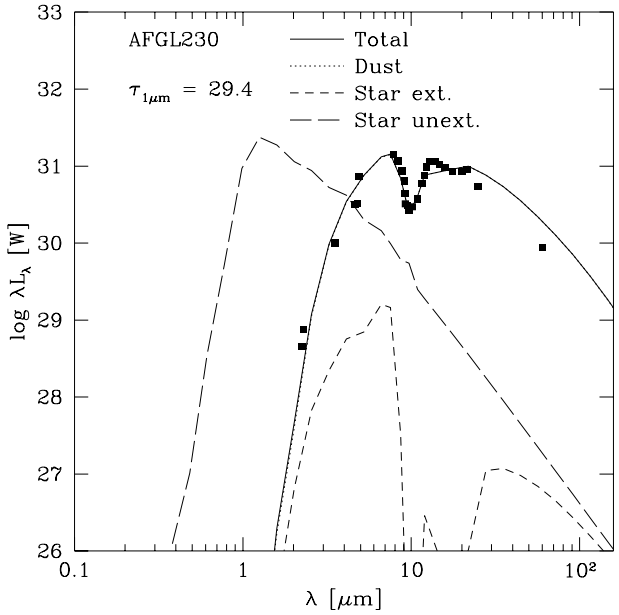

Fig. 1. A fit to the star AFGL230 (data from Justtanont & Tielens 1992). The parameters of the fit are shown in Table 2. Continuous line: emerging spectrum; dotted line, coinciding with the continuous line in this case: dust emission; long dashed line: original photospheric spectrum (T_{eff}=2500 K); short dashed line: extinguished photospheric spectrum.

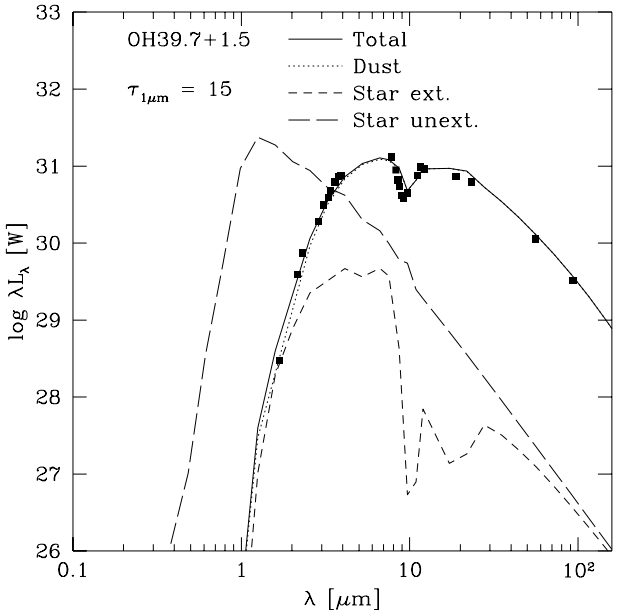

Fig. 2. The same as in Fig. 1 but for OH 39.7+1.5 (data from Bedijn 1987).

Table 2. Model parameters adopted to fit the energy distribution of star AFGL230 and OH 39.7+1.5. The dust mass–loss rate $\dot{M}_d$ ($M_\odot$/yr) has been computed assuming $v_{\rm exp}$ = 15 km/s; r_{in} is in cm and $\rho_{d\ in}$, the corresponding dust density is in g/cm^3.

τ_1	Log(L/L$_\odot$)	Te	r_{in}	$\rho_{d\ in}$	$\dot{M}_d$
			AFGL230		
29.4	4.715	2500	7.1E+14	5.9E-18	8.9E-07
			OH 39.7+1.5		
15.0	4.715	2500	7.1E+14	3.0E-18	4.5E-07

by Granato & Danese (1994) and we summarize here only its main features. The transfer of radiation originating from a central source in an axisymmetric dust distribution is solved with the lambda-iteration method: at each iteration the local temperature of dust grains is computed from the condition of thermal equilibrium with the radiation field estimated at the previous iteration. The convergence is speeded up with respect to this simple scheme following the prescriptions given by Collison & Fix (1991). Moreover, in the present case, taking advantage of the spherical symmetry, the computing times are reduced by about two orders of magnitude. The dust consists in a mixture of different species of grains, which can be specified according to the needs. In this paper, when dealing with OH/IR stars, we use the three silicate grains of the six-grain (three silicates plus three carbonaceous) model defined by Rowan-Robinson (1986) (mixture A). This model provides a very simple but reasonably good description of the absorption law of our Galaxy and of far-IR emission of galactic dust clouds. As for carbon stars, we used the three carbonaceous grains of the same model (mixture B). The characteristics of the dust grains, type, dimension, density, mass fraction and sublimation temperature are displayed in Table 1.

Our numerical code has been widely used in a different context, namely models of dusty tori around AGNs (see Granato et al. 1997 and references therein). Thus it is pretty well tested in the more complex situation where spherical symmetry breaks down. As a further check, we compared our results to the fits provided by other authors to OH/IR stars spectra such as Justtanont & Tielens (1992) and Bedijn (1987). We found a quite good agreement in the fitting parameters (Figs. 1, 2 and Table 2 respectively) even if these authors have often introduced ad-hoc modifications in the optical properties of dust, variable from object to object, with the aim of giving a better description of the strengths and shapes of the 10 and 18 micron silicate features. We stress once again that our purpose is instead to have a good description of the average properties of grains in circumstellar shells.

We will now show that τ_1 can be expressed as a function of known parameters of the star. This result holds true also in presence of a density enhancement (Eq. 2), because the corresponding column density variation is of the order of 10% at most. On the contrary the spectral properties of the envelope depend on both τ_1 and f, but the latter effect requires a detailed modelling that is beyond the scope of the present work. Thus, integrating for the sake of simplicity Eq. 1 from r_{in} to r_{out} we have

$$\tau_1 = \frac{\dot{M}\,\delta\,k_1}{4\pi\,v_{\rm exp}}\frac{1}{r_{in}} \qquad (6)$$

where the term $1/r_{out}$ has been neglected with respect to $1/r_{in}$ and k_1 is the dust opacity at 1 μm. On the other hand the dust sublimation radius is (Granato & Danese 1994)

$$r_{in} = b\, L^{1/2} \tag{7}$$

where the factor b depends mainly on the dust composition (through its melting temperature $\sim$ 1000 K for silicates and $\sim$ 1500 K for graphite), the size distribution and only weakly on the shape of the stellar spectrum. Typical values of b are 2–3×10^{12} for silicates mixture and 1–2×10^{12} for carbonaceous mixture.

Using this equation and Eq. 5 into Eq. 6 we get

$$\tau_1 = \alpha \frac{\dot{M}\, v_{\rm exp}}{L^{1.2}} \tag{8}$$

where v_{exp} is in km/s, $\dot{M}$ in $M_\odot$/yr and L in $L_\odot$. The quantity α, which incorporates the dependence upon k_1 and b, is affected only weakly by the spectrum of the illuminating star. For hot stars emitting mainly in optical UV regime, where the optical properties of dust do not show orders of magnitude variations with the wavelength, the latter dependence would be quite negligible for practical purposes. By converse in our case (cold AGB stars) the situation is a bit less simple. We checked however with the code that adopting $\alpha = 2.32 \times 10^9$ for the silicates mixture and $\alpha = 9.85 \times 10^9$ for the carbonaceous mixture, the errors in τ_1 estimated from Eq. 8 are kept within 5 % for stars with $T_{\rm eff}$ in the range 2500-4000. This is a fair approximation because models with τ_1 differing by less than 5-10 % produce almost identical spectra.

In conclusion, with the machinery described in this section, we computed a sequence of envelope models, providing both the extinction (τ_λ) and emission (D_λ) figures, as a function of τ_1 for two different dust mixtures.

We also derived a relation between τ_1 and the luminosity, the expansion velocity $v_{\rm exp}$ and the mass loss rate $\dot{M}$ of the star. How we obtain these quantities along an isochrone, is described in the next section.

3. The isochrones

To investigate the infrared properties of SSPs we coupled the dusty envelope model described in the previous section with the large library of stellar evolutionary tracks existing in Padova. These tracks are computed for different values of the initial metallicity, keeping constant and equal to the solar partition the relative proportion of the metals. The initial mass of the evolutionary tracks is in the range 0.6 to 120 $M_\odot$ corresponding to ages from few million yr. to several billion yr. Since the main interest of this paper is to focus on the photometric properties of AGB stars, isochrones have been computed only for intermediate age and old stellar populations, thus between say 10^8 yr to $16 \cdot 10^9$yr. The initial chemical composition of the evolutionary sequences adopted here (Bressan at al. 1993 and Fagotto et al. 1994a, b), is [Z=0.004, Y=0.24], [Z=0.008, Y=0.25], [Z=0.02, Y=0.28], and [Z=0.05, Y=0.352], respectively.

The evolution of low mass stars is computed at constant mass and mass loss is applied during the procedure of isochrones construction. The mass-loss rate along the RGB is parameterized by the usual Reimers formulation with η=0.45.

Since the Padova models do not extend into the thermally pulsating AGB phase (TP-AGB), an analytic description is adopted to complete the isochrones up to the phase of the formation of the planetary nebula. We adopt the analytic procedure of Bertelli et al. (1994) which rests on some well defined relations provided by full numerical calculations, namely the core-mass luminosity relation and the reference AGB locus in the Hertzsprung-Russell (HR) diagram as a function of the mass and metallicity of the star (see e.g. VW).

3.1. Mass-loss rate along the AGB

The mass-loss rate along the AGB is a key parameter for the evolution of these stars because it affects the lifetime and the average luminosity of the phase. Both these quantities bear on the contribution of the whole phase to the integrated light because the larger the mass-loss rate the shorter the lifetime of the phase, the dimmer its brightest stars and finally the lower the contribution to the total light of the population. The mass-loss rate also affects the core mass of the subsequent post-AGB stars, hence the ultraviolet properties of the stellar population.

A great effort has been recently devoted to clarify the role of the mass-loss on the evolution of stars along the AGB. It has been shown (Bowen & Willson 1991, VW, Blöcker 1995a, Groenewegen & De Jong 1994, Marigo et al. 1996, 1997) that the mass-loss rate rises almost exponentially with time during the AGB phase and that sooner or later it turns into a superwind that completely evaporates the envelope of the star, leaving a bare core which then evolves toward very high temperatures. All bright AGB stars are known to be variables with amplitudes that may reach about a couple of magnitudes, and infrared observations of Mira and OH/IR stars show the characteristic emission features of a dusty envelope suggesting that pulsations and dust may play an important role in the mass-loss process. However the actual mechanism which drives the mass-loss is still presently not well understood. Moreover mass-loss rate determinations, derived mainly from IR and millimetric measurements, are characterized by a significant uncertainty, related to the unknown distance of the source, the assumed dust to gas ratio and the expansion velocity.

Recent hydrodynamic calculations (Bowen & Willson 1991, Willson et al. 1995) show that the shock waves generated by large amplitude pulsations of AGB stars levitate matter out to a radius where dust grains can condensate; from this point, radiation pressure on grains and subsequent energy redistribution by collisions, accelerate the matter beyond the escape velocity. In this model, the exponential growth of the mass-loss rate is entirely due to the variation of the density scale height below the acceleration region (Bowen & Willson 1991) as the star climbs along the AGB. On the other hand a simple fit to the relation between the mass–loss–rate and the period along with the analytical relations between period, mass, luminosity and effective

temperature of an AGB star (see e.g. VW) show that the mass-loss rate increases exponentially with the luminosity and, above a critical threshold, turns into a superwind limited only by the reservoir of the momentum in the radiation field.

Here we adopt the formalism of VW. Following their empirical relation, the mass loss rate $\dot{M}$ grows exponentially with the pulsation period P until a constant upper limit is reached at a period of about 500 days, which corresponds to the superwind phase. The relation between the mass-loss rate and the period has been derived from observational determinations of mass-loss rates for Mira variables and pulsating OH/IR stars both in the Galaxy and in the LMC. The two regimes are equivalent for a period of about 500 days for the solar composition.

The adopted relations are:

$$\log \dot{M} = -11.4 + 0.0123P \tag{9}$$

Here and in the following, $\dot{M}$ is given in units of $M_\odot$ yr^{-1}, the stellar luminosity L is expressed in $L_\odot$, the pulsation period P in days, c is the speed of light (in km s^{-1}) and $v_{\rm exp}$ (in km s^{-1}) is the terminal velocity of stellar wind.

VW express the mass-loss rate in the superwind phase by equating the final mass momentum flux $\dot{M}v_{\rm exp}$ to the momentum flux of the entire stellar luminosity, according to the radiation-driven-wind theory (Castor et al. 1975):

$$\dot{M} = 6.07023\ 10^{-3}\beta\frac{L}{cv_{\rm exp}} \tag{10}$$

adopting β = 1. While the Galactic OH/IR stars suggest a value of the order unity (Wood et al. 1992), there is no reason why the same value should hold true for other environments such as the LMC because, as clarified by Netzer and Elitzur (1993), the momentum transfer cannot constrain the value of β. Furthermore Wood et al. (1992) found that the expansion velocity is clearly lower in more metal poor stars and concluded that by adopting a constant value for β one would predict that the mass-loss increases at decreasing metallicity, contrary to what is observed.

We thus included a metallicity dependence of the mass-loss rate in the superwind phase by imposing that β scales linearly with the metallicity Z and calibrated this dependence by fitting the infrared spectrum of the OH/IR star TRM 60 in the LMC(Groenewegen et al. 1995). With our envelope model we estimate a value of τ_1 of 8. Assuming a distance modulus for LMC (m-M) $_0$=18.5, the luminosity of the star is 5.4 10^4 L$_\odot$. Since the observed expansion velocity of TRM 60 is 12 km s^{-1} (Wood et al. 1992) we get a dust mass-loss rate of 1.1 10^{-7}M$_\odot$/yr. To convert it in gas mass-loss rate we derive from our scaling law (Eq. 5) a dust to gas ratio of 10^{-3} so that, assuming that this object is in a superwind phase, we get β = 1.13. If we further adopt a metallicity of Z=0.008 for this star (an average value for the LMC) we have:

$$\dot{M} = 6.07023\ 10^{-3}\frac{L}{cv_{\rm exp}} \times 1.13\frac{Z}{0.008} \tag{11}$$

For the Galactic OH/IR stars this relation implies that $\beta \sim 2$, which is a suitable value (Wood et al. 1992).

As far as the expansion velocity is concerned, VW provide the following relation between the velocity $v_{\rm exp}$, (in km s^{-1}) and the period of the star

$$v_{\rm exp} = -13.5 + 0.056P \tag{12}$$

with the additional constraint that $v_{\rm exp}$ is greater than 3 km s^{-1}, a lower limit typical of Mira and OH/IR stars. Furthermore VW constrain the velocity to be less than the average value of 15 km s^{-1}, again a typical value for such stars. However, as shown by Wood et al. (1992), there seems to be a trend between the expansion velocity and the period even for P $\geq$ 500 days (the period corresponding to $v_{\rm exp}$=15 km s^{-1} in the above equation) and, perhaps more important, there seems to be a trend with the metallicity of the star, because the observations suggest that $v_{\rm exp}(LMC)$=0.5-0.6 $\times$ $v_{\rm exp}(Galaxy)$. We thus let the maximum velocity to depend on the period and the metallicity of the star according to the relation

$$v_{\rm exp} \leq 6.5\frac{Z}{0.008} + 0.00226P \tag{13}$$

The slope of this relation has been derived from a linear fit to the data for the Galactic OH/IR stars within 1^o of the Galactic plane (Fig. 6 of Wood et al. 1992), while the metallicity dependence of the zero point rests on the assumption that the few data for the LMC OH/IR stars in the same figure obey the same relationship, however scaled to a lower metallicity Z=0.008 instead of Z=0.02.

Finally the pulsation period P is derived from the period-mass-radius relation (see Eq. 4 in VW) which is obtained by assuming that variable AGB stars are pulsating in the fundamental mode:

$$\log P = -2.07 + 1.94\ \log R - 0.9\ \log M \tag{14}$$

where the period P is given in days and the stellar radius R and mass M are expressed in solar units.

A final comment concerns the validity of the core-mass luminosity relation, which has been assumed here as one of the relations adopted to compute the analytic TP-AGB phase. It is well known that hot bottom burning in stars of initial mass larger than about 4 M$_\odot$ causes a brightening of about 20% with respect to the usual core-mass luminosity relation. However the above effect disappears when the star reaches the superwind phase (see e.g. VW) which is the most relevant for the present purpose. We also neglected the modulation of the luminosity introduced by thermal pulses (e.g. Marigo et al. 1996, 1997) on the notion that also this effect constitutes a higher degree of approximation which is beyond the current scope as we need to keep only a minimum number of free parameters at work.

3.2. The PAGB stars

As a consequence of the superwind phase the star eventually reaches a maximum luminosity after which it loses most of its envelope and rapidly evolves toward the so called Post-AGB

path (PAGB). Thereafter the star reaches a maximum temperature at almost constant luminosity and then it cools and dims along the White Dwarf cooling sequence. The observed initial-final mass relation of PAGB stars (Weidemann 1987) constitutes a further test for the AGB phase and supports the kind of mass-loss rate adopted here (VW, Bertelli et al. 1994)

PAGB stars have been suggested as one of the main contributors to the integrated ultraviolet light of nearby elliptical galaxies. In the bulge of M31 their estimated contribution to UV light amounts to $\simeq 20\%$. However in M32 their number per unit UV light, as seen from the same HST FOC 1550 optical combination, is an order of magnitude lower. This indicates that age and metallicity effects may significantly affect the contributions of the PAGB stars that are ultimately related to the AGB evolution.

Characteristic evolutionary paths of PAGB stars of different mass and composition have been computed by Paczyński (1971), Schönberner (1981), Iben (1984), Blöcker & Schönberner (1991), Fagotto et al. (1994) and Blöcker (1995b). For the present isochrones we assembled the data from Schönberner (1981), Blöcker & Schönberner (1991), Fagotto et al. (1994), and Blöcker (1995b).

4. Isochrones in the Infrared

Transformations from the theoretical to the observational plane were performed by making use of the stellar spectral library of Bressan et al. (1994), Silva (1995) and Tantalo et al. (1996). The core of the spectral library is the atlas by R. Kurucz (1993). At temperatures higher than $T_{\rm eff}$ = 50,000 K pure black-body spectra are adopted, whereas for stars cooler than $T_{\rm eff}$ = 3500 K the catalog of stellar fluxes by Fluks et al. (1994) is implemented. The latter library is based on stars of solar metallicity ($Z \sim 0.02$) whereas the library of SSPs presented here spans the range of metallicity $0.004 \leq Z \leq 0.05$. To account for a dependence on the metal content even for M giants, we adopted the same library at different metallicities but assigned the spectral class, identified by the (V-K) color, adopting the (V-K)-$T_{\rm eff}$ relation of Bessell et al. (1991) which depends on the metallicity.

To account for the effect of dust along the TP-AGB we proceed in the following way. For a given temperature, luminosity, mass and metallicity, making use of Eqs. 8 (and 3, when required), we derive the value of τ_1 and interpolate in our sequence of envelope models, obtaining both the extinction (τ_λ) and emission (D_λ) figures. The characteristic stellar spectrum is then modified according to the relation

$$F_\lambda = F_\lambda \times e^{-\tau_\lambda} + D_\lambda \times L \tag{15}$$

where the first factor in the RHS represents the extinction while the second one represents the dust emission. A final renormalization of the whole spectrum to the σT^4 relation is performed but it usually amounts to a negligible correction, indicating that the whole procedure is sufficiently accurate.

Before proceeding further we compare our results with the infrared colors of Mira and OH/IR stars and discuss the reliability of our selected circumstellar envelope models. Fig. 3 shows several isochrones of 1.5 Gyr and different metal content in the two color IRAS diagram, superimposed to the sample of IRAS sources defined by Van der Veen & Habing (1988). The original sample includes about 1400 sources for which $[60]-[25] < 0$ and $[25]-[12] < 0.6$, these limits define the regions occupied by galactic late type stars in the IRAS two color diagram. In the above notation $[\lambda_2]$-$[\lambda_1]$=log($F_{\lambda_2}/F_{\lambda_1}$). However, in order to minimize contamination by cirrus emission, we excluded all the sources with cirr3/F(60)>2 (Ivezic and Elitzur, 1995). The sample plotted in Fig. 3 reduces to about 300 sources.

A thorough discussion of this diagram together with the regions occupied by galactic Mira and OH/IR stars can be found in Habing (1996). Fig. 3 reports data and models in form of magnitudes. Theoretical IRAS monochromatic fluxes were obtained by convolving the stellar spectral energy distributions with the proper transmission curve as detailed in Bedijn (1987). IRAS magnitudes were thus derived according to

$$M_i = -2.5 \times Log(S_i) + 2.5 \times Log(S_{0_i}) \tag{16}$$

where S_i is the flux in Jansky and the constants S_{0_i} are derived from the IRAS PSC-explanatory supplement (1988) and are 28.3 Jy, 6.73 Jy, 1.19 Jy and 0.43 for the 12, 25, 60 and 100 μm passband respectively. This procedure is adopted to facilitate the construction of mixed optical-IR two color diagrams as described below.

Turning now to Fig. 3 we notice that, before reaching the AGB phase, the isochrones are confined in a small region delimited by two open circles, with both (m12-m25) and (m25-m60) $\simeq$0. These figures correspond to the Rayleigh-Jeans spectral regime and indicate that this approximation is fairly accurate till the most advanced phases of the isochrone, where dust comes into play. As the star reaches the thermally pulsating AGB phase the effect of mass-loss suddenly increases and the circumstellar envelope starts to modify the spectral emission. The first envelope model corresponds to τ_1=0.01 and it is indicated by a filled square at (m12-m25) $\simeq$0.6 and (m25-m60) $\simeq$-0.1 for the case of the silicate mixture and by a filled triangle at (m12-m25) $\simeq$0.2 and (m25-m60) $\simeq$0.35 for the carbonaceous mixture, respectively.

Fig. 3 depicts isochrones of different metallicity but they are barely distinguishable in this diagram. This is because our envelope models are characterized by a single parameter, the optical depth, so that different conditions resulting in the same value of τ_1, such as metallicity, mass-loss rate and expansion velocity, provide the same dust envelope and in turn give rise to the same overall spectrum. In contrast, a noticeable feature of this diagram is the dispersion of the data. Ivezic & Elitzur (1995) thoroughly discussed this problem and they were able to show that the bulk of the data are delimited by the τ_1 curves corresponding to grains of either pure silicates or graphite. The thick dashed line in Fig. 3 refers to an isochrone we computed accounting for carbonaceous grains only, characteristic of C rich stars, and it is meant to illustrate the effects of the variation of the chemical composition of the dust. Thus we confirm the results of Ivezic & Elitzur (1995). Fig. 3 also depicts the path an AGB star would follow during a shell ejection of 0.02 $M_\odot$,

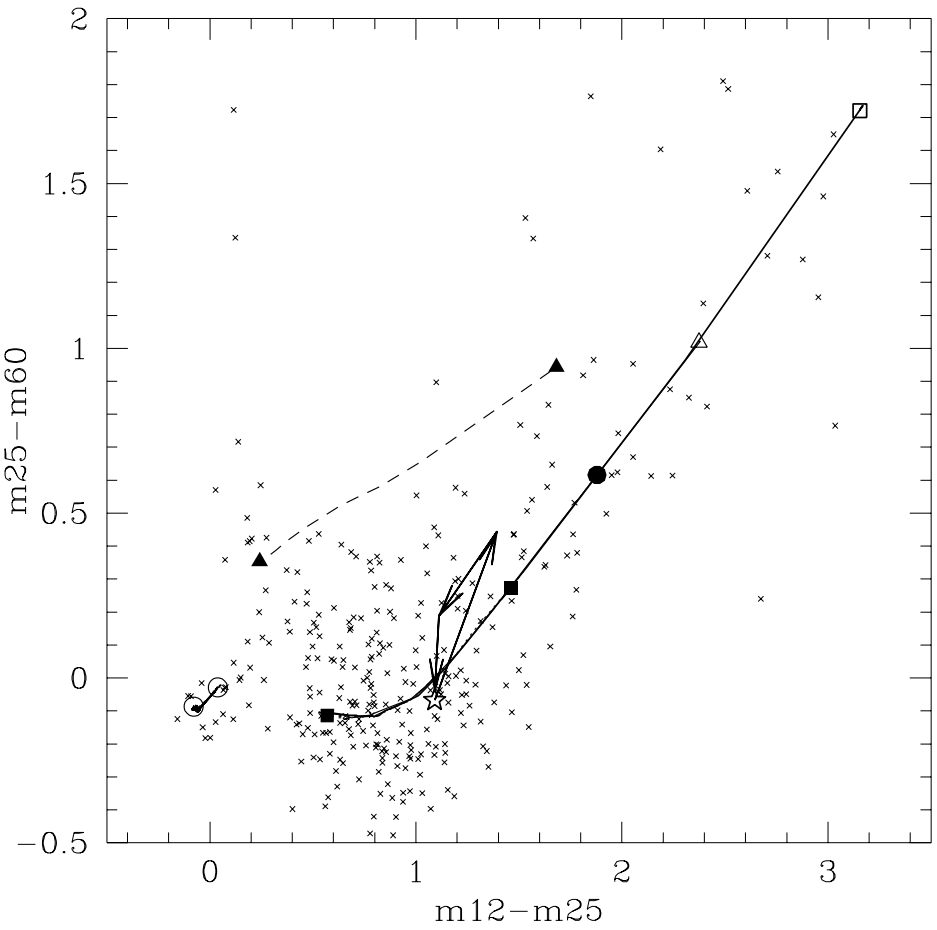

Fig. 3. Two color diagram of the sample of IRAS sources defined by Van der Veen & Habing (1988). Following Ivezic and Elitzur (1995) the sources with cirr3/F(60)>2 have been excluded in order to minimize contamination by cirrus emission. Superimposed are 1.5 Gyr isochrones of different metallicity and a model of an AGB star with T_{eff}=2500K, LogL/$L_{\odot}$=4, τ_1=1 and $v_{\rm exp}$=15 km/s (empty star), surrounded by an expanding shell of 0.02$M_{\odot}$ at 0.2, 0.5 and 0.8 r_{out} (arrows). See text for more details.

and it is meant to illustrate additional effects possibly at work which however, are difficult to predict on the basis of simple stellar parameters.

It is remarkable that isochrones of different metallicity and age reach different maximum values of τ_1. The larger the metallicity the higher the value of τ_1 and the further the isochrone extends in the IRAS two color diagram. The largest value of τ_1 reached by models of different metallicity are indicated in Fig. 3 by a filled square (τ_1=4.4), a filled circle (τ_1=11.1), an open triangle (τ_1=22.3) and an open square (τ_1=57.5) for the metallicity Z=0.004, Z=0.008, Z=0.02, Z=0.05 respectively. The filled triangle at (m12-m25) $\simeq$1.7 and (m25-m60) $\simeq$0.9 refers to the case of Z=0.02 and a mixture of carbonaceous dust grains (τ_1=99).

In summary, while we analyzed both the case of a different mixture and a shell enhancement, we consider the ability of our simple models to reproduce the bulk of the data in the IRAS two color diagram as a meaningful test of reliability, also in view of the errors on the quoted fluxes ($\simeq$ 5%) reported in the IRAS PSC-explanatory supplement (1988).

To check the behavior of our models in the near infrared region of the spectrum, we have also compared our isochrones with a sample of M giants and Miras in the Southern Polar Cap, for which Whitelock et al. (1994, 1995) obtained J, H, K and L magnitudes. Fig. 4 shows the two color (J-H)–(H-K) diagram of M giants (filled squares) and Miras (filled triangles) in the Southern Polar Cap (Whitelock et al. 1994, 1995) superimposed to some selected isochrones at different age and metallicity. Both the bulk of the M giants at (J-H) $\simeq$1 and (H-K)$\simeq$0.3 and those of Miras sample are well reproduced by the models. The fit to the latter sample however depends on the adopted temperature scale, in particular to the temperature assigned to the more advanced M spectral types of the Fluks atlas. Only by reaching the most advanced spectral types during the superwind phase we are able to match the Miras in Fig. 4, as can be seen from the location of our adopted M giant spectra (large filled circles in the figure). Assigning a metallicity on the basis of the isochrone fitting of near infrared colors is thus a quite delicate process, whose reliability must be clearly improved by more accurate atmospheric models. Note that in our case the bulk of Mira stars are well fitted by models of solar metallicity, while it is impossible to assign a metallicity to the M giants. Finally notice that the highly reddened data are relatively well fitted by our dusty models. On the contrary isochrones based on pure photospheric models would never be able to fit the data, as can be seen from the location of late type giants of our spectral library.

Fig. 5 is analogous to Fig. 4 but for the colors (J-K)–(K-L). Here the fit to the Mira sample is poor, suggesting that the problem for the latter stars may be related to the adopted atmospheric models (see also Bessell et al. 1991 and Whitelock et al. 1994).

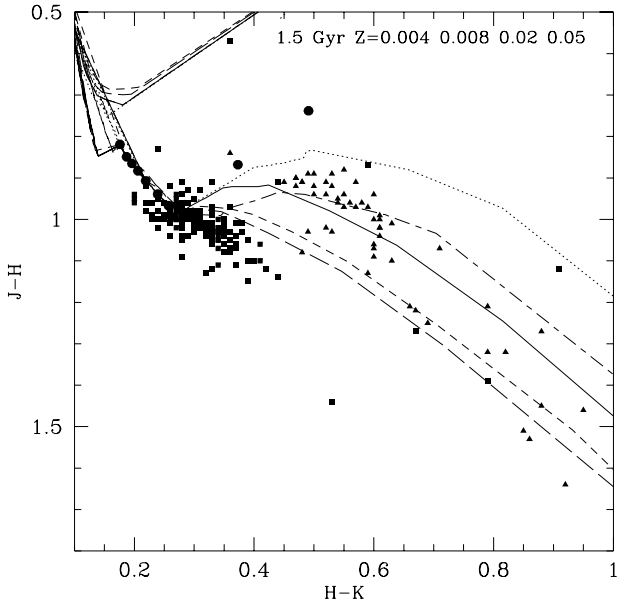

Fig. 4. (J-H)-(H-K) two color diagram of a sample of galactic M (squares) and Mira (triangles) stars from Whitelock et al. (1994, 1995). Superimposed are some selected isochrones of 1.5 Gyr with metallicity Z=0.004 (long-dashed line), Z=0.008 (short-dashed line), Z=0.02 (continuous line) and Z=0.05 (dotted line) for the mixture A, and Z=0.02 (long-short dashed line) for the mixture B. Large filled dots indicate the location of the adopted M giant atmospheric models.

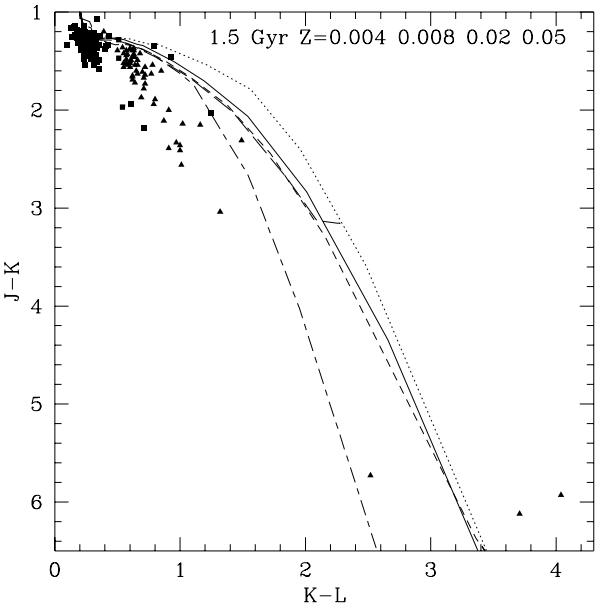

Fig. 5. Same as in Fig. 4 but for the (J-K) and (K-L) colors

However, as in the previous case, the fit improves significantly at high optical depth.

5. Integrated colors: the age-metallicity degeneracy

Once the spectrum of a single star is obtained it is weighted by the appropriate number of stars in the elemental interval of the isochrone and summed up to obtain the integrated spectrum of the SSP. Throughout this paper we adopted a Salpeter initial mass function

$$\phi(M)dM \propto M^{-x}dM \tag{17}$$

with x=2.35. The integration is performed from M_{inf}=0.15 up to the largest initial mass which still contributes to the integrated spectrum of the isochrone.

5.1. Integrated spectra

The integrated spectra F_ν vs. λ in μm of SSP of 0.2 1.5 and 5 Gyr are shown in Fig. 6. In each panel three cases are depicted. In the standard SSP (dot-dashed line) the effects of dusty circumstellar envelopes around Mira and OH/IR stars are neglected. In the other two cases the circumstellar envelopes have been included in modelling the AGB phase. The continuous line refers to the mixture of silicate grains (mixture A) and it is well suited for an AGB dominated by M giants, while the dashed line represents models computed with the mixture of carbonaceous grains (mixture B) and should be more appropriate for a population rich in C-stars. In the latter case the mid infrared spectra are featureless as it is expected from the optical properties of the carbonaceous grains (note however that our mixture do not include PAH molecules, whose possible formation in the photosphere of C-stars is discussed by Helling et al. 1996).

Differences with respect to the standard SSP appear beyond a few μm where the contribution of the brightest AGB stars to the integrated light of the stellar population is large. After a decrease of the flux in the region from 1 to 3 μm because the brightest stars are heavily obscured by their circumstellar envelopes, at larger wavelengths the contribution of the dust dominates, reaching an order of magnitude at 10 μm over the pure photospheric models. While there are clear differences between the two selected dust mixtures, they constitute a modulation over the main effect brought about by the inclusion of the dust in the envelope. At increasing age the relative contribution of AGB stars to the integrated light decreases and, correspondingly, the inclusion of a proper circumstellar envelope becomes less and less important.

Metallicity effects are depicted in Fig. 7 where we plot SSPs of 3 Gyr for Z=0.008, Z=0.02 and Z=0.05 as indicated in the corresponding panels. It can be noticed that the dust emission progressively shifts toward larger wavelengths as the metal content increases, indicating that the spectra are dominated by cooler dust envelopes. The metallicity affects the properties of the dust envelope through Eq. 8. By combining this equation with Eq. 11, describing the super-wind phase, it is easy to show that the optical depth of the envelope is a linear function of the metallicity Z and the maximum value of τ attainable at a given metallicity scales as $L^{-0.2}$. Thus in the superwind phase, more metal rich isochrones are characterized by a larger value of the optical depth. Moreover at a given metallicity, older isochrones reach a larger value of the maximum optical depth, but this ef-

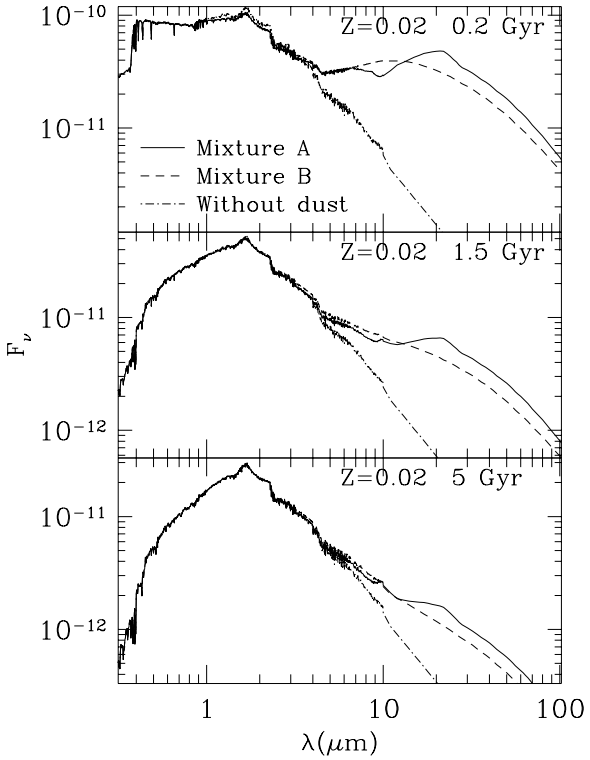

Fig. 6. Integrated spectrum F_ν vs. λ in μm of SSPs of 0.2 Gyr 1.5 Gyr and 5 Gyr and solar composition. Three cases are depicted. In the first case dust is not taken in to account (dot-dashed line), in the second dust is a mixture of silicates grains (continuous line), and in the third dust is a mixture of carbonaceous grains (dashed line).

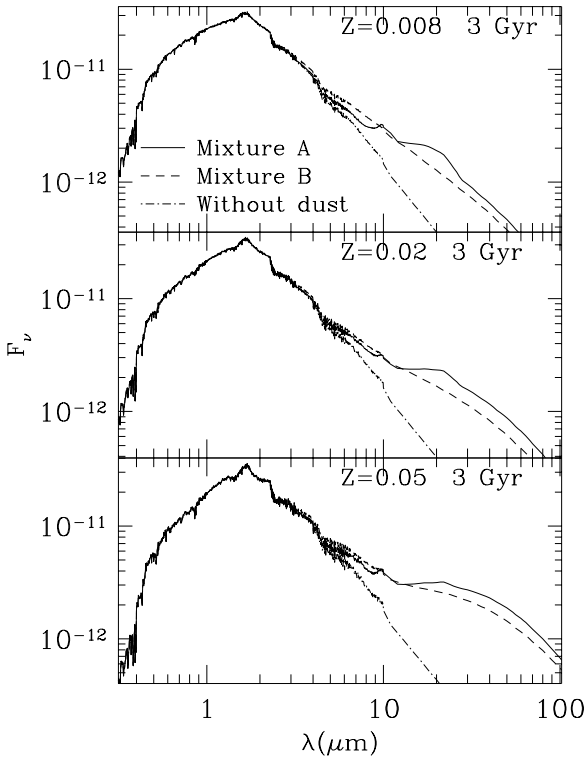

Fig. 7. The same as in Fig. 6 but for a fixed age of 3 Gyr and metallicity Z=0.008, Z=0.02 and Z=0.05, respectively.

fect is compensated by the lower contribution of the AGB phase to the integrated light of the population.

5.2. Integrated colors

Accurate analysis of the integrated properties of SSPs at optical wavelengths have been done in a number of recent studies (Bertelli et al. 1994, Bressan et al. 1994, Tantalo et al. 1996, Charlot et al. 1996). Fig. 8 depicts optical and near IR two color plots of SSPs at different age and metallicity and reveals one of the major problems encountered when working with integrated properties: age and metallicity vectors are almost superimposed in these diagrams and it is virtually impossible to disentangle the two effects. In particular, because one of the applications of the concept of SSP is concerned with the age derivation of early type galaxies, this means that once a set of observed colors or narrow band indices are fitted with models of a given metallicity, there is always the possibility that either a younger but more metal rich population or an older but more metal poor one provides an equally acceptable fit. This effect has been known for a long time and it is the main source of uncertainty in deriving absolute ages of early-type galaxies (Bressan et al. 1994, Gonzales 1993 , Charlot et al. 1996). Therefore finding a pair of indices whose age and metallicity behavior is orthogonal, would allow a separation of these effects and would provide an unambiguous estimate of both the age and metallicity of a complex stellar system.

Worthey et al. (1994) were able to show that one such pair is provided by H_β and MgFe indices. In the plane defined by H_β and MgFe indices the field elliptical galaxies analyzed by Worthey et al. occupy a narrow band characterized by a small range in MgFe (an index mainly related to the global metallicity) and a range in H_β corresponding to a significant dispersion in age (from 15 to few Gyr). Bressan et al. (1996) however pointed out that the H_β index is very sensitive to recent episodes of star formation that may have interested only a tiny fraction of the galaxy mass, so that the age of the bulk of the population is still inaccessible through this method, implying that our view of the evolution of these objects still remains obscure. The degeneracy has a major impact on the age determination of the high redshift galaxies, since one of the major challenges offered by nowadays observations is to look at galaxies when their age is only a fraction of that of the universe. Bender et al. (1995) measured narrow band indices of early-type galaxies in clusters down to redshift z $\leq$0.3 finding that those systems are compatible with only a passive evolution of their stellar populations. Recently Franceschini et al. (1997a) combining HST magnitudes with JHK and ISO 6.7 μm magnitude for a typical early-type galaxy in the Hubble Deep Field at redshift z$\simeq$1 concluded that the bulk of the stellar population is about 4 Gyr old and as massive as 4×10^{11} $M_\odot$. A major episode of star formation must have occurred at redshift z = 1 + Δ z_{4Gyr}, which for a flat universe

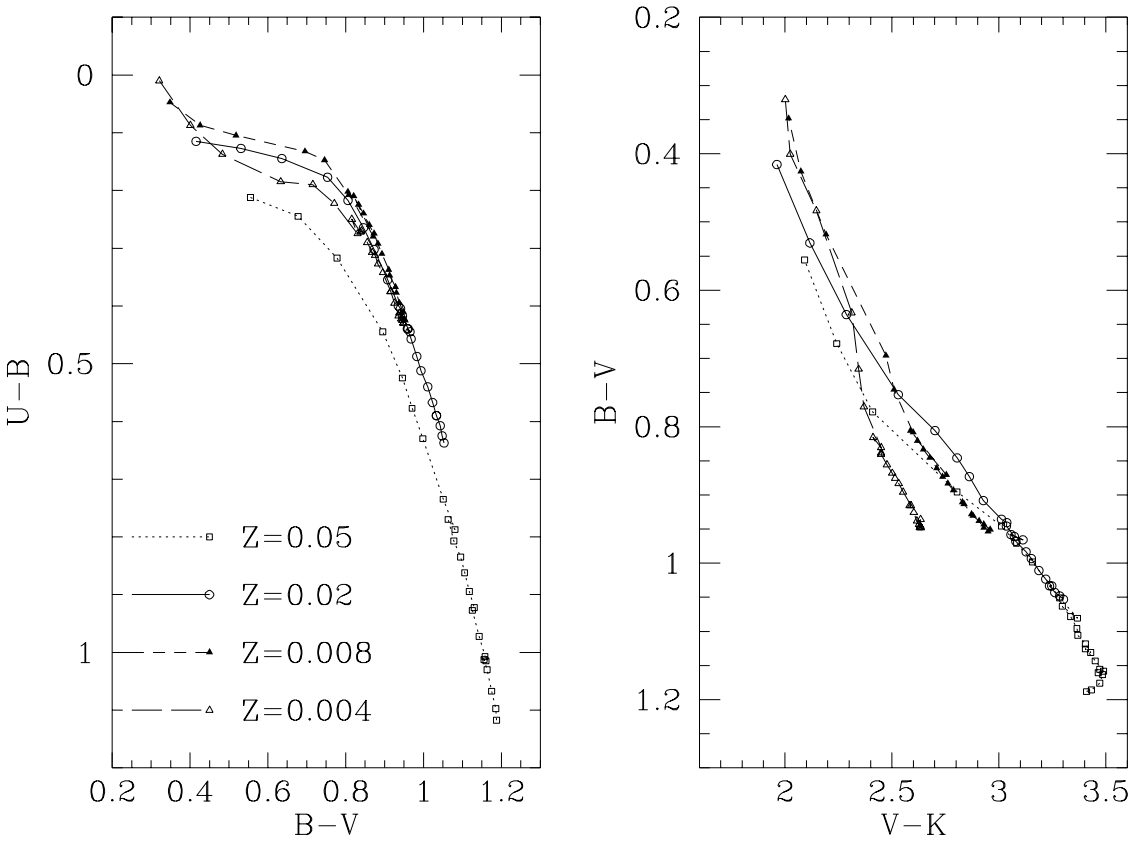

Fig. 8. Optical and near infrared two color diagrams of SSPs at varying age and metal content illustrating the problem of the age-metallicity degeneracy. Age runs from 0.5 Gyr (top left) to 15 Gyr (bottom right) in steps of 0.5 Gyr up to 7 Gyr and thereafter in steps of 1 Gyr.

and H_0=50 km/s/Mpc corresponds to z$\geq$5 and for an open Ω=0 universe and H_0=50 km/sec/Mpc to z$\geq$2.5. Our new SSP models show that adopting a metal content larger by about the 50% would decrease the age from 4 Gyr to about 2 Gyr, and the corresponding formation redshift would be z$\leq$2 in both cases. While the obvious settling of the problem is on a statistical basis, this example clearly illustrates a feasible test for the models of galaxy formation. Indeed, solar or even larger metallicities, as suggested by local observations of narrow band indices and ultraviolet upturn (Bressan et al. 1994, 1996) in elliptical galaxies and ages of few Gyr as determined by fitting the broad band colors of intermediate redshift objects, constitute the space of parameters where the AGB population keeps its maximum effect upon the integrated star light and it is possible that, because of the effect of the dust, the new SSP models are most indicated for solving the age metallicity degeneracy, provided that suitable pass-bands are selected.

To illustrate the point, Fig. 9 and Fig. 10 show combined optical, near IR and mid IR two color diagrams of several SSPs computed adopting the silicate mixture. The 6.7μm and 15μm magnitudes are obtained by adopting a zero point flux of 94.7 Jy and 17 Jy respectively and have been selected for comparison with ISO data. Fig. 9 depicts the run of the color (V-K) against the color (K-6.7) for different metallicities (Z=0.004, 0.008, 0.02 and 0.05) and some selected ages. Above 1.5 Gyr the different sequences are well separated, with leftmost sequence corresponding to the lowest metal content and the rightmost one corresponding to Z=0.05. At intermediate ages the effect of the metallicity is clearly at odd with that of the age because AGB stars drive the mid IR fluxes of the composite populations. Younger isochrones are bluer in the (V-K) color but redder in the (K-6.7) due to the effect of the dust, while more metal rich isochrones are redder in both colors. This causes the breaking of the age-metallicity degeneracy. Such a behavior can be compared with that of optical and near infrared colors in order to appreciate the power of the diagnostic tool we are suggesting. Plotting the (V-K) color against (K-15μm) or (K-25μm) would provide similar results, so that the corresponding figures are not shown here for sake of conciseness.

The (V-6.7) vs. (6.7-15) two color plot (upper panel of Fig. 10) is also a suitable diagnostic diagram. Note that there is a variation of more than half a magnitude in the (V-6.7) color going from Z=0.004 to Z=0.02 at intermediate ages. In contrast, optical colors change by less than 0.1 mag in the same age range. Plotting an optical magnitude (e.g. V) seems required in order to obtain useful diagnostic diagrams. Indeed inspection of intermediate age SSPs show that while optical, near and mid IR absolute magnitudes display the same trend with the age (they increase by about one magnitude going from 2 to 6 Gyr, irrespective of the metallicity), they behave differently with re-

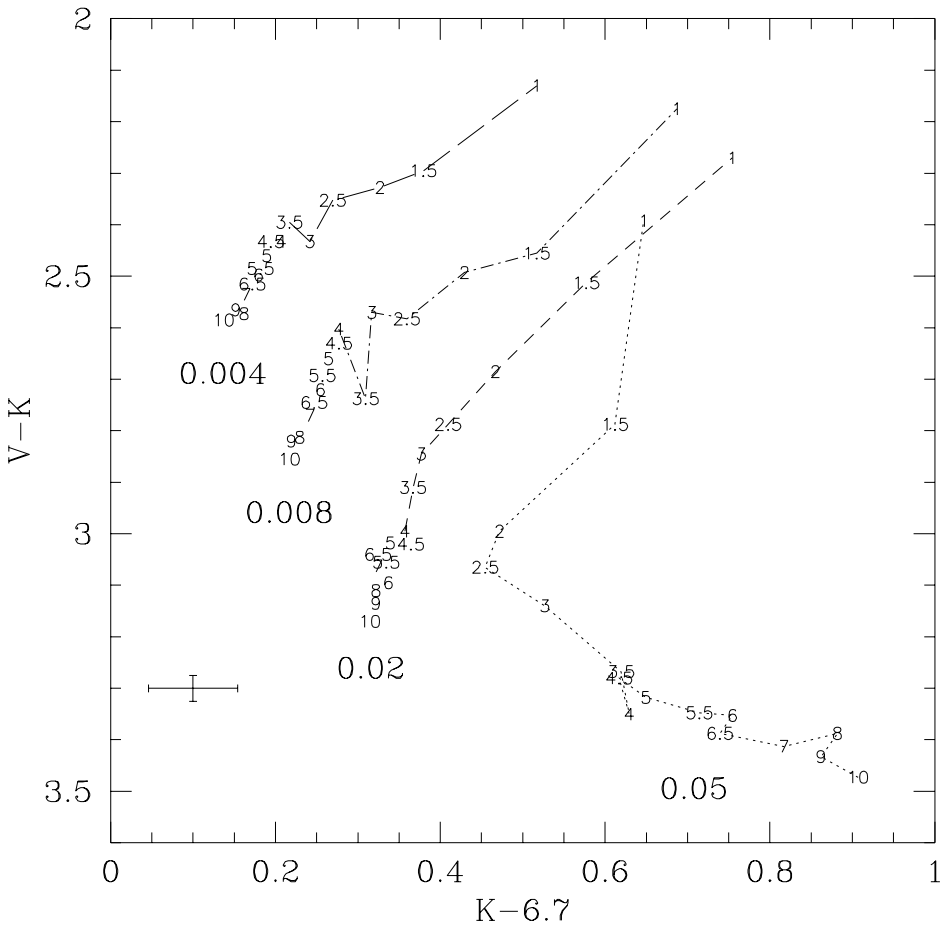

Fig. 9. A mixed optical (V), near (K) and mid (6.7μm) infrared two color diagram of SSPs. The metallicity Z is indicated in the figure. Numbers along the curves indicate the age in Gyr. The error bar corresponds to a 5% and 10% uncertainty in the flux measurement in the near and mid IR respectively. Due to dust effects in the envelope of AGB stars, age and metallicity differences may be fairly well recognized in intermediate age populations.

spect to the metallicity. Optical magnitudes become fainter as the metallicity increases, but the trend inverts when near IR bands are considered and at 6.7μm, 15μm and 25μm there is a remarkable brightening with the metallicity (dust makes the SSP more bright at increasing metallicity). The lower panel of Fig. 10 contrasts the (K-6.7) color instead of the (V-6.7) one. Disentangling age and metallicity effects becomes now more difficult, because the fluxes in the selected passbands show the same behavior with respect to the metallicity.

While both the (V-K) vs. (K-6.7) and the (V-6.7) vs. (6.7-15) two color plots seem well suited for the purpose of disentangling age and metallicity effects, some cautionary notes are necessary at this point.

First of all we have *assumed* a linear dependence on the metallicity of the fraction of the momentum carried out by radiation responsible for the dust acceleration in the superwind phase. This affects, in particular, τ_1 for the most metal rich populations and it is responsible of the odd behavior of the corresponding models in the two color plots. Such a relation should be tested against forthcoming ISO observation of AGB stars.

Furthermore, SSPs with different dust mixture display different IR spectra (Figs. 6 and 7); in particular the SSPs with the silicates mixture show features around 10-20 μm. Leaving aside the problem of the dust composition in real cool stellar envelopes, it is clear that the relative percentage of O-rich and C-rich stars may affect the mid IR shape of the integrated spectrum. When an O star becomes a C star (III dredge-up) and eventually turns again into an O star (hot bottom burning), and how it depends on the metallicity of the environment is still a matter of debate. We neglected transient phenomena such as shell ejection or luminosity dip, that may also affect the infrared colors of the star (e.g. Fig. 3). Detailed modelling of such effects is underway (Marigo et al., in preparation).

Some sort of dilution due to a range in age and metal content should be present in the spectrum of a composite system, however this could be of minor importance for early type galaxies if low metallicity stars are practically absent (Bressan et al. 1994) and the formation time is short, as suggested by the observed enhanced composition (Bressan et al. 1996, Tantalo et al. 1997).

Finally, environmental effects should be considered when adopting these models to interpret the colors of galaxies. The presence of a low level star formation activity could mask the infrared AGB emission. But the opposite is also true: the models indicate that the mid IR emission of an intermediate age population alone is up to an order of magnitude larger than predicted by pure photospheric models. Also the presence of a diffuse gas phase, the cirrus component, could dominate the galactic spectrum beyond 20 μm. All these phenomena are the subject of a forthcoming investigation (Silva et al. 1997).

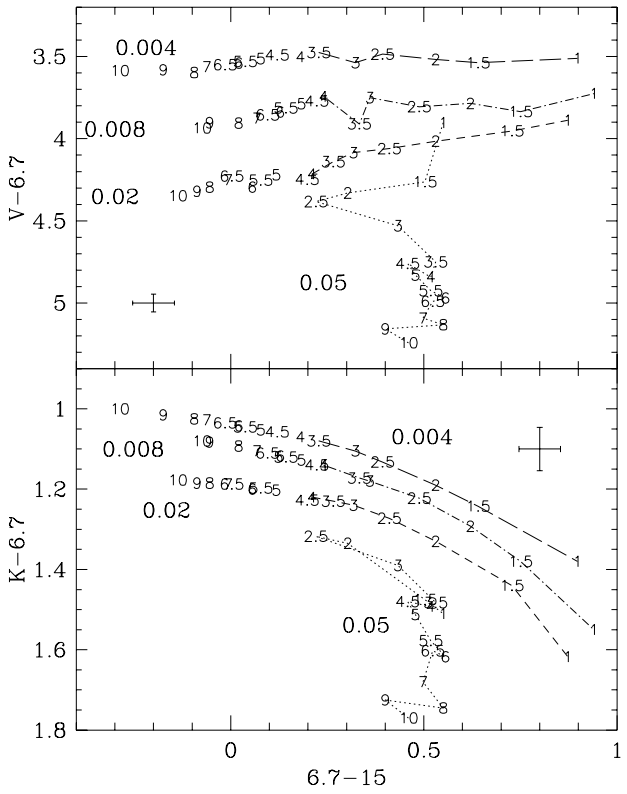

Fig. 10. The same as in Fig. 9 but for the (V-6.7μm) and (6.7μm-15μm) colors, and (K-6.7μm) and (6.7μm-15μm) colors.

6. Conclusions

In this paper we modelled the infrared emission of late type stars surrounded by a steady-state outflows of matter driven by radiation pressure on dust grains. To this aim we solved the radiative transport equations inside a spherically symmetric stationary flow of matter, in order to derive the extinction and the emission of the dust as a function of the wavelength. Several envelope models were constructed as a function of the optical depth of the envelope τ_1, a suitable scaling parameter for the models (see also Ivezic & Elitzur 1995). We also found a relation between this scaling parameter τ_1 and the mass-loss rate, expansion velocity, luminosity and metallicity. Finally by adopting some empirical relations we could express this quantity as a function of the basic stellar parameters, mass, luminosity effective temperature and metal content, in such a way that we could assign the suitable dust envelope to the stars along the AGB.

We thus computed isochrones at different ages and metallicity where, for the first time, the effect of the dust envelope around the brightest AGB stars is accounted for in a consistent way. Comparing our isochrones with the sample of IRAS sources defined by Van der Veen & Habing (1988) in the two color diagram we run into the problem of the dispersion of the data perpendicularly to the sequence defined by different value of τ_1. We briefly discuss the possibility of overcome this difficulty by adopting a different grain mixture or by allowing the occurrence of a density enhancement caused by an outward expanding shell. While both these effects can account for the mentioned dispersion, we considered the ability of our stationary models to fit the bulk of the data in the IRAS two color diagram as a good test of reliability, and adopted these models to compute the integrated properties of the SSP.

As a further test we compared our isochrones with a sample of galactic M and Mira stars from Whitelock et al. (1994, 1995). In the near infrared colors (J-H vs. H-K) the models fit nicely both the M giants and the Miras. Models without the effect of dust cannot fit the location of the Mira stars, as indicated by the location in this diagram of our adopted model atmospheres. Apparently the sample of Mira stars is best fitted by models with solar metallicity, however this conclusion is much dependent on the adopted temperature scale of the more advanced M spectral types other than by the atmospheric model itself. Forthcoming ISO observations would certainly help in clarifying this point.

Existing studies based on theoretical SSP either do not account for the effect of dust in the envelope of bright AGB stars or they simply give a rough estimate of the effect and, consequently, neither class of models is fully suitable for investigating the integrated properties of stellar systems in the infrared (Charlot et al. 1996). In our present calculations the mass-loss along the AGB determines both the lifetime and the spectral properties of the stars, allowing the description of the whole phase inside a consistent framework.

The direct effect of the metallicity is included by a simple parameterization of the superwind mass-loss rate, which finally provides the scaling parameter τ_1. However the metal content also affects the effective temperature of the AGB phase and consequently the mass-loss rate determined by the empirical relation with the pulsational period.

Effects of AGB stars show up even in the integrated spectrum of the population, at wavelength above few μm where they are the largest contributors to the integrated light. At these wavelengths integrated spectra computed without the effect of dust envelopes are about one order of magnitude fainter than the models including Miras and OH/IR stars. This effect decreases as the SSP becomes older and older.

We show that by selecting suitable passbands, the integrated colors of such new SSPs can potentially be used to disentangle age from metallicity effects because of the strong dependence of the dust model on the metal content. However given the short duration and the high luminosity of the phase this method will suffer of a great stochastic effect when applied to systems with a relatively small number of stars (Chiosi et al. 1988, Santos & Frogel 1997). These stochastic effects would certainly constitute less of a problem in the interpretation of the integrated light of large systems such as the nuclei of elliptical galaxies or the spiral bulges. These considerations suggest that incoming infrared observations of intermediate redshift objects could be the targets where this method will eventually exploit its maximum capability.

Finally, the new SSP models will be included in a more extended study aimed at modelling the spectral properties of the galaxies from the ultraviolet to the far infrared, accounting for the effects of the dust associated with star forming regions and

with the diffuse interstellar gas (Silva et al. 1997, Franceschini et al. 1997b)

Acknowledgements. We thank Paola Marigo, Alberto Franceschini and Leo Girardi for helpful discussions. We also thank our referee, A. Lançon for her useful comments and suggestions. This research was supported by the European Community under TMR grant ERBFMRX-CT96-0086

References

Bedijn P. J. 1987, A&A 186, 136
Bender R., Ziegler B., Bruzual G. 1996, ApJ 463, 51
Bertelli G., Bressan A., Chiosi C., Fagotto F., Nasi E. 1994, A&AS 106, 275
Bessell M.S., Wood P.R., Brett J.M., Scholtz M., 1991, A&AS 89, 335
Blöcker T. 1995a, A&A 297, 727
Blöcker T. 1995b, A&A 299, 755
Blöcker T., Schönberner D. 1991, A&A 244, L43
Bowen G.H., Willson L.A. 1991, ApJ 375, L53
Bressan A., Fagotto F., Bertelli G., Chiosi C. 1993, A&AS 100, 647
Bressan A., Chiosi C., Fagotto F. 1994, ApJS 94, 63
Bressan A., Chiosi C., Tantalo R. 1996, A&A 311, 425
Castor J.J, Abbot D.C., Klein R.I. 1975, ApJ 195, 157
Charlot S., Worthey G., Bressan A. 1996, ApJ 457, 625
Chiosi C., Bertelli G., Bressan A. 1988, A&A 196, 84
Collison A.J., Fix J.D. 1991, ApJ 368, 545
Elitzur M., Goldreich P., Scoville N. 1976, ApJ 205, 384
Fagotto F., Bressan A., Bertelli G., Chiosi C. 1994a, A&A 104, 365
Fagotto F., Bressan A., Bertelli G., Chiosi C. 1994b, A&A 105, 369
Fluks M.A., Plez B., The P.S. at al. 1994, A&AS 105, 311
Franceschini A., Bressan A., Granato G.L. et al. 1997a, in ESA SP-401
Franceschini A., Silva L., Granato G.L., Bressan A., Danese L. 1997b, ApJ, submitted
Freedman W. 1992, AJ 104, 1349
Fusi Pecci F., Renzini A. 1976, A&A 46, 447
Goldreich P., Scoville N. 1976, ApJ 205, 144
Gonzales J.J. 1993, Ph. D. thesis, Univ. California, Santa Cruz
Granato G.L., Danese L. 1994, MNRAS 268, 235
Granato G.L., Danese L., Franceschini A. 1997, ApJ 486, 147
Groenewegen M.A.T., De Jong T. 1994, A&A 283, 463
Groenewegen M.A.T., Smith C.H., Wood P.R., Omont A., Fujiyoshi T. 1995, ApJ 449, L119
Habing H.J. 1996, A&AR 7, 97
Habing H.J., Tignon J., Tielens A.G.G.M. 1994, A&A 286, 523
Helling C., Jorgensen U.G., Pletz B., Johnson H.R. 1996, A&A 315, 194
Iben I.J. 1984, ApJ 277, 333
IRAS Science Team, 1988, IRAS PSC explanatory supplement
Ivezic Z., Elitzur M. 1995, ApJ 445, 415
Justtanont K., Tielens A.G.G.M. 1992, ApJ 389, 400
Kurucz R.L. 1993, Kurucz CD-ROM, Cambridge, MA: Smithsonian Astrophysical Observatory, December 4, 1993
Marigo P., Bressan A., Chiosi C. 1996, A&A 313, 545
Marigo P., Bressan A., Chiosi C., 1997 A&A accepted
Netzer N., Elitzur M. 1993, ApJ 410, 701
Paczyński B. 1971, Acta Astron. 21, 417
Rowan-Robinson M. 1986, MNRAS 219, 737
Salpeter E.E. 1974a, ApJ 193, 579
Salpeter E.E. 1974b, ApJ 193, 585
Santos J. F. C. Jr., Frogel Jay A. 1997, ApJ 479, 764
Schönberner D. 1981, A&A 103, 119
Silva L., 1995, Degree thesis, Univ. Padova, IT
Silva L., Granato G.L., Bressan A. & Danese L. 1998, ApJ, submitted
Tantalo R., Chiosi C., Bressan A., Fagotto F. 1996, A&A 311, 361
Tantalo R., Bressan A., Chiosi C. 1997, A&A submitted,
Van Der Veen W.E.C.J., Habing H.J. 1988, A&A 194, 125
Vassiliadis E., Wood P.R. 1993, ApJ 413, 641
Weidemann V. 1987, A&A 188, 74
Willson L.A., Bowen G.H., Struck C. 1995, BAAS 187, 103.18
Whitelock P., Menzies J., Feast M. et al. 1994, MNRAS 267, 711
Whitelock P., Menzies J., Feast M. et al. 1995, MNRAS 276, 219
Wood P.R., Whiteoak J. B., Hughes S. M. G et al. 1992, ApJ 397, 552
Worthey G., Faber S.M., Gonzalez J.J., Burstein D. 1994, ApJS 94, 687

This article was processed by the author using Springer-Verlag LaTeX A&A style file *L-AA* version 3.